## PAPER

Check for updates

# Influence of protonic acid on the structure and properties of poly(3,4-ethylenedioxythiophene):poly(styrenesulfonate) in oxidation polymerization

Jialin Guo,[a] Kai Zhang, [ID]*[ab] Piao Luo,[a] Nanjie Wu,[a] Shigui Peng, [ID][a] Lanlan Wei,[b] Yufei Liu,[a] Min He,[ab] Jie Yu,[ab] Shuhao Qin,[ab] Qiao Fan,[a] Tingting Luo[a] and Jun Xiao [ID][b]

Poly(3,4-ethylenedioxythiophene):poly(styrenesulfonate) (PEDOT:PSS) is widely used because of its excellent performance. We report the synthesis of two PEDOT:PSS dispersions. The two dispersions differ by the addition of additional protonic acid in the oxidative polymerization system. Although there are examples of the introduction of acids into the polymerization system, the effects of acid on the structure and properties of these materials, in particular their mechanisms of action, have not been elucidated. We describe the chemical structure and molecular weight of two PEDOT polymers using Fourier transform infrared spectroscopy, X-ray photoelectron spectroscopy, UV-vis-NIR spectroscopy, and density functional theory calculations. The carrier concentration, carrier mobility, and surface morphology of the composites are characterized by UV-vis-NIR spectroscopy, electron spin resonance, Raman spectra, Hall effect measurements, and atomic force microscopy. The crystallinity of PEDOT:PSS was measured by X-ray diffraction patterns. We show that the addition of a proper amount of protonic acid to the oxidative polymerization system can effectively reduce the formation of the terminal carbonyl group of PEDOT chains, which is conducive to the growth of polymer chains, and further improve the carrier concentration, which leads to an improvement of conductivity. Our results highlight the optimization of the chemical structure of PEDOT in order to increase its molecular weight and ultimately its conductivity.

## 1. Introduction

Poly(3,4-ethylenedioxythiophene) (PEDOT) is widely used in energy storage, sensors, coatings, organic effect transistors, photovoltaic cells, and OLED devices due to its outstanding electrical conductivity, excellent environmental stability, and high transmittance in the visible range.[1–10] However, the application of PEDOT is limited because it is insoluble, infusible, and difficult to process. In order to solve this problem, water-soluble polystyrene sulfonate (PSS) was used as the dispersant and counterion dopant of PEDOT in water,[11,12] and PEDOT:PSS dispersions with excellent film-forming properties were synthesized. The initial synthesis of PEDOT:PSS results in a relatively low-conductivity polymer, although it has excellent performance and wide application. Therefore, it is a well-known key problem to improve the conductivity of PEDOT:PSS. There are many ways to improve the conductivity of PEDOT:PSS, which can be divided into three categories according to the treatment methods:

(1) Solvent addition treatment:[13–20] the conductivity of PEDOT:PSS can be greatly improved by doping its dispersion with polar solvent or acid. For example, dimethyl sulfoxide (DMSO), ethylene glycol (EG), protonic acid, and the like are common PEDOT:PSS dopants. In that PEDOT:PSS dispersion system, the dopant can play a role in dope which refers to improving the chain oxidation degree of the PEDOT, inducing PEDOT aggregation or enabling the planar conformation of the PEDOT to be converted into a quinoid structure from a benzene structure;

(2) Film post-treatment:[14,21–25] acid treatment, especially protonic acid treatment, can weaken the coulomb attraction between PEDOT and PSS, resulting in the formation of phase separation morphology, which is conducive to the removal of insulating PSS. This further results in better crystallization of PEDOT in the film, which exhibits high electrical conductivity;

(3) Optimize that synthesis process: in the polymerization process of PEDOT:PSS, PEDOT can be optimized by adjusting the molecular weight of PSS, the EDOT:PSS ratio, the oxidant, the catalyst and the acidity of the polymerization system.

[a]*Department of Polymer Material and Engineering, College of Materials and Metallurgy, Guizhou University, Guiyang, China. E-mail: k.zhang2008@qq.com*
[b]*National Engineering Research Center for Compounding and Modification of Polymeric Materials, Guiyang, China*

Different molecular weights of PSS bring different charge mobility and transconductance.[26,27] Moreover, differences in oxidants can lead to large differences in the oxidation state of the PEDOT polymer.[28–32] Controlling the amount of monomer and catalyst can control the initial polymerization rate and then control the linear degree of PEDOT, which affects the conductivity of PEDOT:PSS.[33] When the acidity of the EDOT:PSS polymerization system is sufficient, it will lead to a series of effects, such as EDOT terminal protonation, PSSH/PSSNa content change and so on, which will affect the linear conformation of PEDOT, thus affecting the conductivity, work function, colloidal stability, and other properties of PEDOT:PSS.[32,34,35]

Wherein the protonic acid is involved in the three treatment methods. There was no change in the chemical structure or molecular weight of PEDOT, either by film post-treatment or by solvent addition. Both of the two treatments are carried out on the basis that the polymer dispersion system has already been formed. The introduction of protonic acid into polymer synthesis has been studied, but the mechanism of its role in the synthesis process is still unclear. Therefore, it is very important to explore the mechanism of protonic acid in the synthesis process.

In this work, we studied the change in the polymerization mechanism of EDOT in the oxidative polymerization system of EDOT:PSS in the presence of protonic acid. Sulfuric acid was directly added to the oxidative polymerization system of EDOT:PSS, and EDOT was polymerized in the presence of sulfuric acid. The structure, molecular weight, oxidation degree, carrier concentration, carrier mobility, conformation, and microstructure of PEDOT:PSS dispersion and films were characterized by Fourier transform infrared (FTIR), UV-vis-NIR absorption spectrum, DFT calculations, X-ray photoelectron spectroscopy (XPS), Raman spectra, electron spin resonance (ESR), atomic force microscope (AFM) images, Hall effect measurements and X-ray diffraction (XRD) patterns. This study provides guidance to optimize the structure of EDOT in the oxidative polymerization route, which is beneficial to the preparation of highly conductive PEDOT:PSS materials.

## 2. Experimental

### 2.1 Materials

PSS ($M_w \sim$ 75 000, 30 wt% in $H_2O$) was obtained from Shanghai Macklin Biochemical Technology Co., Ltd. (China). EDOT, sodium persulfate, potassium *tert*-butoxide, ferric sulfate, sulfuric acid, dimethyl sulfoxide (DMSO), sulfuric acid and dimethyl sulfoxide (DMSO) were purchased from Shanghai Aladdin Biochemical Technology Co., Ltd. (Shanghai, China). Ion exchange resin was obtained from Ningbo Zhengguang Resin Co., Ltd. (Ningbo, China).

### 2.2 Preparation of PEDOT:PSS dispersions and films

Two sets of PEDOT:PSS dispersions, designated S1 and S2, were prepared.

S1: 1.60 g of PSS, 0.45 g of sodium persulfate, 0.02 g of ferric sulfate and 39 g of deionized water were added into a closed reaction vessel and stirred until the solid was dissolved. Then,

0.22 g of EDOT was added thereto, and the mixture was stirred at a speed of 500 rpm for polymerization for 24 hours. After completion of the reaction, 12 g of ion exchange resin was added, followed by further stirring at 400 rpm for 6 hours and filtration to obtain the PEDOT:PSS dispersion S1.

S2: 1.60 g of PSS, 0.35 g of concentrated sulfuric acid, 0.45 g of sodium persulfate, 0.02 g of ferric sulfate and 39 g of deionized water were added into a closed reaction vessel and stirred until the solid was dissolved. Then, 0.22 g of EDOT was added thereto, and the mixture was stirred at a speed of 500 rpm for polymerization for 24 hours. After completion of the reaction, 12 g of ion exchange resin was added, followed by further stirring at 400 rpm for 6 hours and filtration to obtain the PEDOT:PSS dispersion S2.

The PEDOT:PSS dispersion was taken out a plurality of times by using a glue head dropper and dropped on a glass sheet with a smooth surface, and then the dispersion liquid was uniformly distributed on the surface of the glass sheet by adopting a scraping method. The PEDOT:PSS films were dried in a blast drying oven at 80 °C for 15 minutes to obtain uniformly dried PEDOT:PSS films.

### 2.3 Characterization

The conductivity of the film was measured using a FT-330 four-point probe method. And the film thickness was measured by a Carl Zeiss LSM900 laser confocal microscopy. The UV-vis-NIR absorption spectrum of the films was measured using a Shimadzu UV-3600i Plus UV-vis-NIR spectrophotometer. Fourier transform infrared (FTIR) of the film was measured in the range of 400 $cm^{-1}$ to 4000 $cm^{-1}$ using a Nicolet IS50 Fourier transform infrared (FT-IR) spectroscopy. The XPS spectra was obtained from a Thermo Scientific K-Alpha X-ray photoelectron spectrometer. The Raman spectra in the range of 50 $cm^{-1}$ to 4000 $cm^{-1}$ were obtained by using Horiba LabRAMH REvolution system made in Japan and 785 nm Ar + laser as excitation source. The carrier concentration and carrier mobility of the films were measured by Ecopia Hall effect tester HMS-7000. Electron spin resonance (ESR) was measured using a Bruker EMXplus-6/1 X-band spectrometer. Atomic force microscope (AFM) images were obtained from a 1500001N atomic force microscopy. X-ray powder diffraction patterns of PEDOT:PSS were acquired using an advanced diffractometer (Thermo Scientific ARL EQUINOX 3000) in a continuous scanning mode with monochromatic Cu-Kα, $I$ = 40 mA, and $U$ = 40 kV. Sample detection was performed in an air atmosphere, and the sample was irradiated in the $2\theta$ range from 2 to 100°. The relationship between the number of monomer units and the energy gap of PEDOT was studied at DFT using Gaussian, based on keywords: opt freq b3lyp/6-31+g(d,p) geom = connectivity.

## 3. Results and discussion

### 3.1 Chemical structure analysis of PEDOT

Two PEDOT:PSS dispersions were synthesized by oxidative polymerization. The first group is the sample synthesized by the initial formula, named S1. Then the second group is the sample

synthesized under the condition of adding sulfuric acid into the system before the reaction and is named S2. The PEDOT:PSS dispersions S1 and S2 were made into thin films on glass substrates.

According to Fig. 1, $Fe^{3+}$ catalyzes the decomposition of persulfate to generate peroxy radicals during the oxidative polymerization of EDOT or during the growth of PEDOT oligomer chains. Peroxy radicals further react with EDOT monomers to form reactive EDOT cationic radicals, which trigger the continuous polymerization of EDOT and eventually generate PEDOT long chains.[32] The existence of protonic acid in the PEDOT polymerization system will produce a protonic

acceleration effect.[32,36] Whether the protonic acid will affect the chemical structure of PEDOT in the polymerization process is worth discussing and studying. According to the infrared spectrum analysis of Fig. 2(a), it was found that S1 had a very obvious absorption peak at 1730 $cm^{-1}$, while S2 had no obvious absorption peak at this position. The absorption peak represents that PEDOT with carbonyl end groups in the system, indicating that the PEDOT end groups were blocked by the carbonyl group.[37] From the XPS spectra, different states of carbon in S1 and S2 were detected, as shown in Fig. 3. As a result, as shown in Table 1, the ratios of the carbonyl peak areas of S1 and S2 were 4.98% and 3.59%, respectively. Both FT-
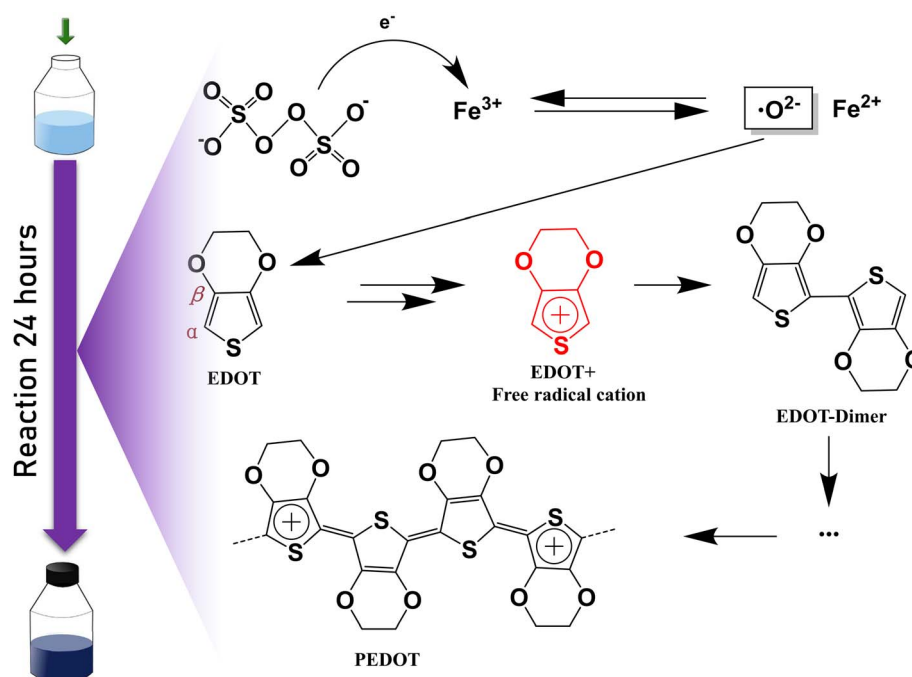


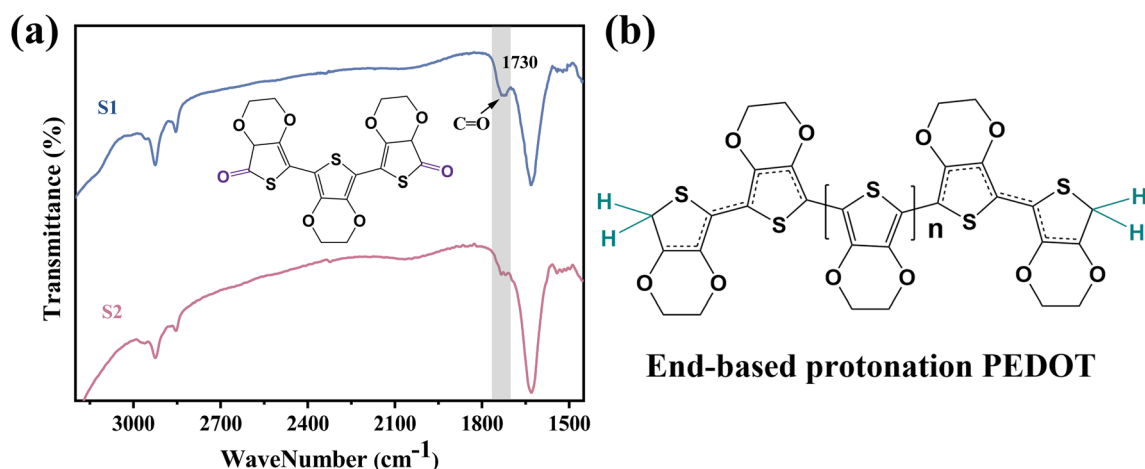**Fig. 1** Oxidation polymerization route of PEDOT.



**Fig. 2** (a) FTIR spectra of the PEDOT:PSS without sulfuric acid and with sulfuric acid. The structural formula in the figure is PEDOT with end groups blocked by carbonyl groups. (b) End-based protonation PEDOT chain.
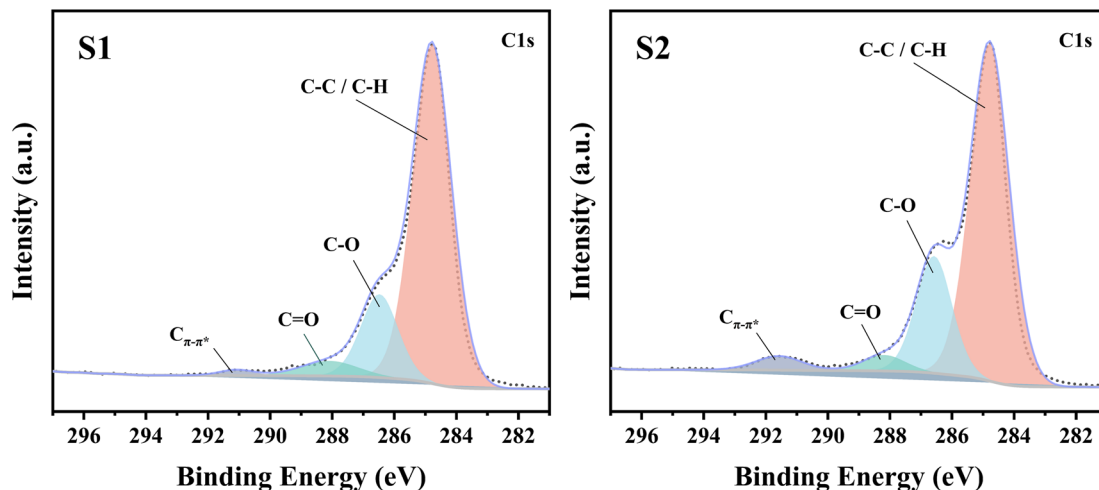
**Fig. 3** XPS C(1s) spectra of PEDOT:PSS films S1 and S2.

**Table 1** Comparison between the proportions of different states of carbon in S1 and S2

| Type of carbon state | S1 | S2 |
|---|---|---|
| C–C/C–H | 75.95% | 70.37% |
| C–O | 17.97% | 22.55% |
| C=O | 4.98% | 3.59% |
| $C_{\pi-\pi^*}$ | 1.11% | 3.49% |

IR and XPS spectra showed that the addition of sulfuric acid during the oxidative polymerization of PEDOT resulted in a decrease of PEDOT with carbonyl end groups. The EDOT or PEDOT radical intermediates in the polymerization were easily altered due to the presence of oxygen during the reaction. The product was no longer an EDOT or PEDOT radical intermediate. As shown in Fig. 2(b), the addition of protonic acid during EDOT polymerization has been shown to result in protonation of the PEDOT chain end groups.[35] Hydrogen attacked the $C_\alpha$ of the EDOT or PEDOT end groups and preferentially occupied this position, thus weakening the access of oxygen to the end groups, which protected the $C_\alpha$.

Hydrogen attacks the $C_\alpha$ of the EDOT or PEDOT end group, preferentially occupying that position and thereby reducing the carbonyl-attached end group, which protects the $C_\alpha$ for further polymerization. Therefore, we analyzed the molecular weight of PEDOT:PSS indirectly. It is well known the UV-vis-NIR absorption spectrum can be used to analyze the relative molecular weight of PEDOT because the absorption spectrum of neutral PEDOT will redshift with the increase of monomer units.[38,39] Usually, the synthesized PEDOT is in the oxidation state, also known as the polaron state and the bipolaron state. However, the characteristic highest occupied molecular orbital-lowest unoccupied molecular orbital (HOMO–LUMO) transition of PEDOT can only be detected in the neutral state.

Firstly, a potassium *tert*-butoxide-DMSO strong reduction system was used for carrying out reduction de-doping treatment

on the PEDOT:PSS to convert the PEDOT:PSS in an oxidation state into a PEDOT:PSS film in a neutral state. Secondly, the UV-vis-NIR absorption spectrum was collected, and the results were shown in Fig. 4(a). As expected, S1 and S2 exhibit strong absorption peaks in the range of 500 nm to 700 nm, corresponding to the π–π* transition in the PEDOT main chain, indicating that neutral PEDOT is obtained.[39,40] According to Fig. 4(a), the absorption peak of S1 is at 629 nm, and the absorption peak of S2 is at 650 nm. It can be clearly seen that the absorption peak of S2 in the neutral state wavelength range is significantly shifted in the high wavenumber direction relative to S1, which indicates that the molecular weight of PEDOT in S2 is significantly larger than that in S1.

The interaction between the PEDOT cell segment and its neighbors results in the formation of an electron band. The highest occupied molecular orbital, referred to as homo, is an analog of the valence band (V.B.) in metals and semiconductors, while the lowest unoccupied molecular orbital (LUMO) corresponds to the conduction band (C.B.). The two bands are separated by a forbidden band called the energy gap.

According to eqn (1):

$$E = c \times h/\lambda \tag{1}$$

where $E$ represents energy, $c$ represents the speed of light, $h$ represents Planck's constant, and $\lambda$ represents wavelength. There is a certain correlation between the wavelength of the ultraviolet absorption spectrum and the HOMO/LUMO gap, as shown in Fig. 4(b). As shown in Fig. 4(c), by DFT calculations, we obtain the HOMO/LUMO gap corresponding to different PEDOT monomer unit numbers. Then the linear equations of the monomer unit number of the HOMO/LUMO gap and PEDOT are obtained.[41] On the basis of this relationship, the HOMO/LUMO gap energy corresponding to the maximum absorption peak 629 nm of S1 is 1.97 eV, and the HOMO/LUMO gap energy corresponding to the maximum absorption peak 650 nm of S2 is 1.90 eV. Owing to the linear equation obtained by fitting, the HOMO/LUMO gap energy of 1.97 eV for S1
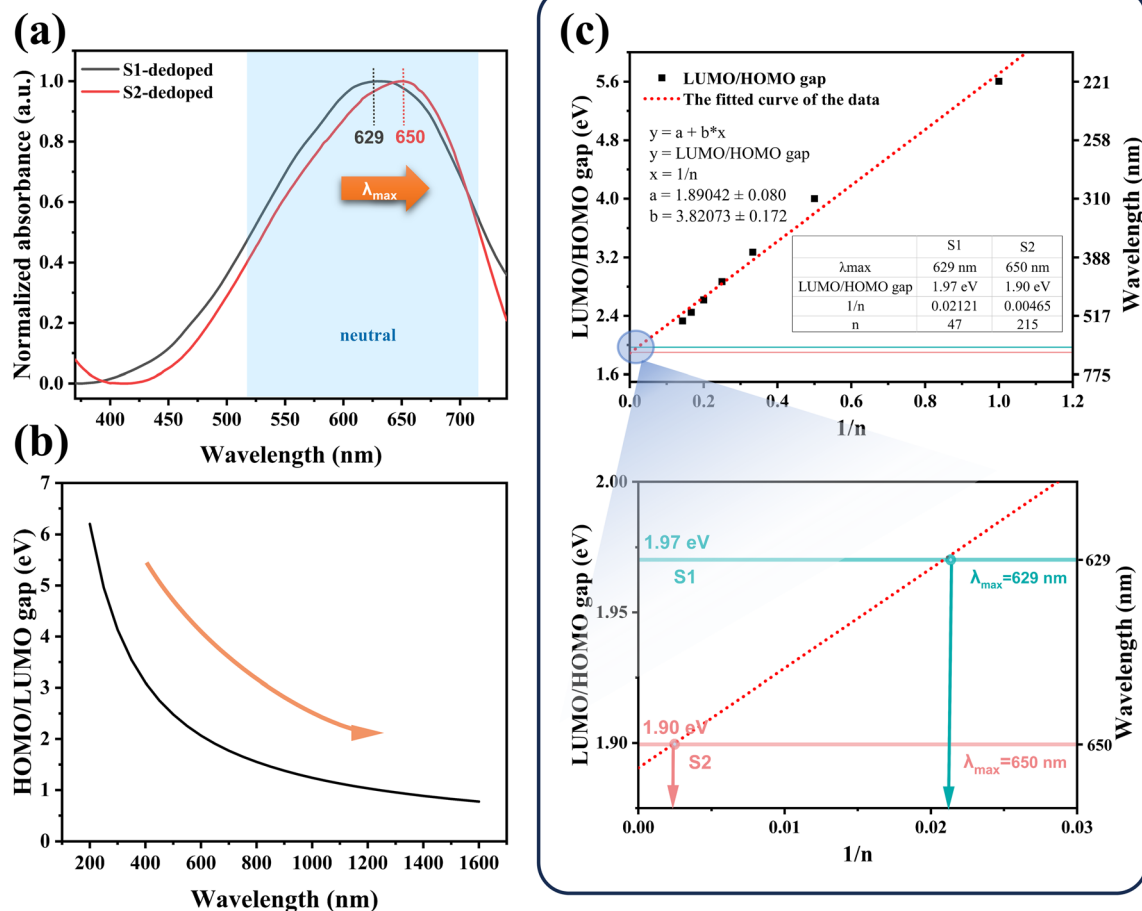
**Fig. 4** Characterization and theoretical calculation of PEDOT molecular weight. (a) UV-vis-NIR absorption spectra of the dedoping PEDOT:PSS without sulfuric acid and with sulfuric acid. (b) The HOMO/LUMO gap-wavelength curve. There is a correlation between HOMO/LUMO gap of PEDOT and wavelength of the UV-vis-NIR absorption spectra. (c) The HOMO/LUMO gap-1/$n$ curve. The "$n$" refers to the number of monomer units of PEDOT.

corresponds to 47 PEDOT monomer units, while that of S2 is 215. The molecular weight of PEDOT obtained here is only a theoretical value, and there must be some deviations in the calculation process, but the calculation process provides a method basis for further accurate PEDOT molecular weight.

## 3.2 Carrier concentration and mobility analysis of PEDOT:PSS

For the PEDOT:PSS material itself, its electrical conductivity is as follows:

$$\sigma = ne\mu \tag{2}$$

where $\sigma$ represents conductivity, $n$ represents carrier concentration, $e$ is unit charge, and $\mu$ is carrier mobility. The factors affecting the conductivity of PEDOT:PSS include carrier concentration and carrier mobility.

We first analyze the difference in carrier concentration between the two samples. The carrier concentration of PEDOT, which may also be referred to as the degree of oxidation, includes polaron concentration and bipolaron concentration.

The oxidation of PEDOT generates a new electronic state in the band gap, which transforms the material from a nearly insulating or low-conductive state to a metalloid or high-conductive state. The energy difference between the band edge and these newly introduced states depends on the band gap as well as the chain length of the polymer.[42]

In addition, in the case of the same PEDOT chain length, we speculated that the oxidation degree of the terminal protonated chain was higher and the oxidation state was more stable than that of the unprotonated chain, except that the terminal protonation of PEDOT chains would bring different molecular weights and then affect its oxidation state.

For this reason, we detected the oxidation degree of PEDOT:PSS. A UV-vis-NIR spectrum of the synthesized untreated PEDOT:PSS films is measured, and the result is shown in Fig. 5(a). In the UV-vis-NIR absorption spectrum, PEDOT with a higher oxidation level shows strong absorption in the high wavenumber range. According to those different oxidation levels, the UV-vis-NIR absorption spectrum is divided into three wave band ranges according to the different oxidation levels of PEDOT, namely a neutral state region, a polaron
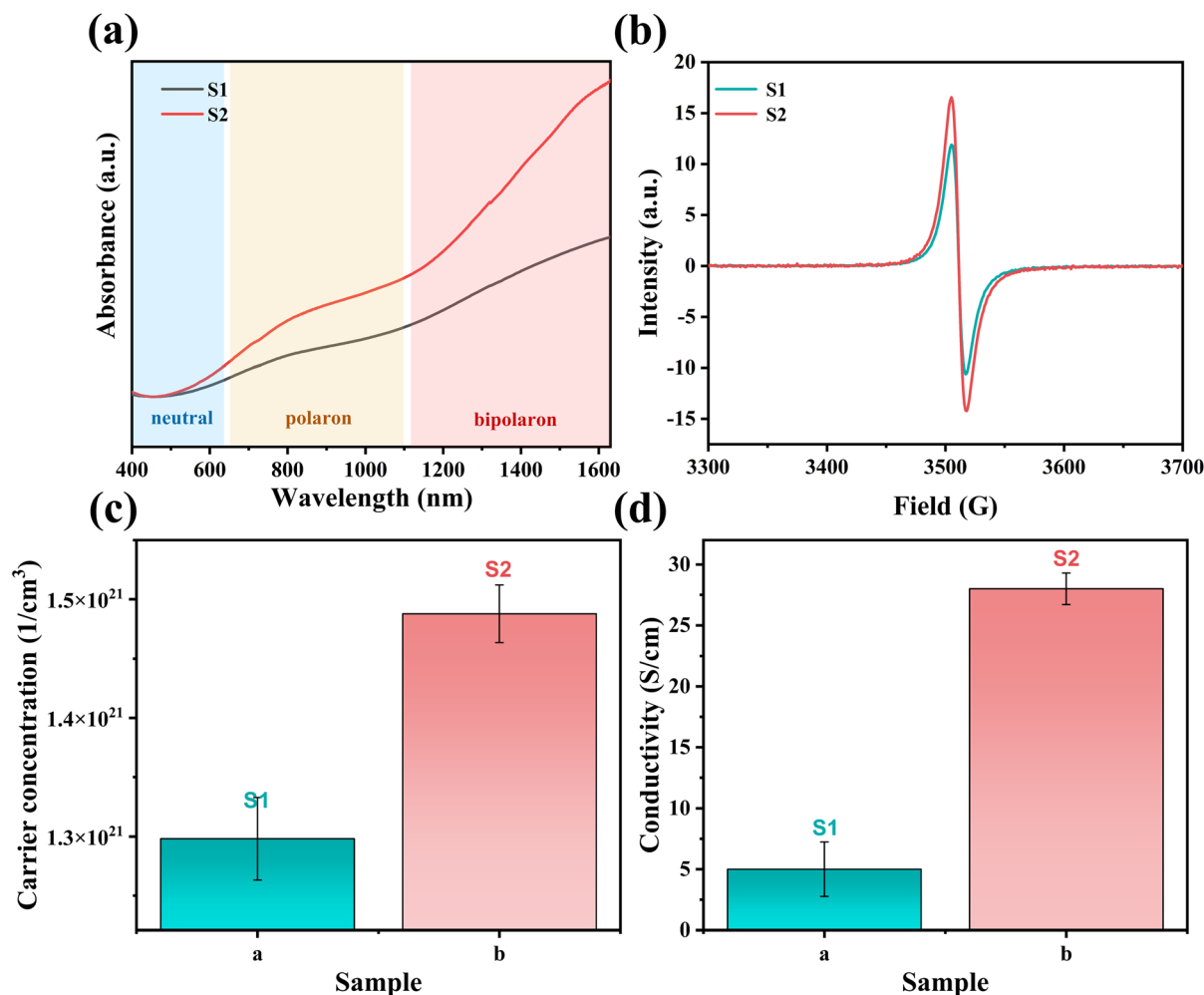
Fig. 5 (a) UV-vis–NIR absorption spectra of the PEDOT:PSS without sulfuric acid and with sulfuric acid. (b) ESR spectra of the PEDOT:PSS without sulfuric acid and with sulfuric acid. (c) Carrier concentration of the samples without sulfuric acid and with sulfuric acid. (d) Conductivity of the samples without sulfuric acid and with sulfuric acid.

region, and a bipolaron region,[43,44] as shown in Fig. 5(a). The result shows that the absorption intensity of S2 is obviously higher than that of S1 in the UV-vis–NIR absorption spectrum region representing the polaron state, and the difference is more obvious in the bipolaron region. As shown in Fig. 5(b), the polaron concentrations of S1 and S2 were obtained by the ESR test. The test results show that the signal intensity of S2 is higher than that of S1, which indicates that the polaron concentration of S2 is higher. The carrier concentration (the sum of the polaron and bipolaron concentrations) and the carrier mobility of the PEDOT:PSS were measured using a Hall effect tester. As shown in Fig. 5(c), the carrier concentrations in S1 and S2 were measured to be $1.29 \times 10^{21}$ cm$^{-3}$ and $1.48 \times 10^{21}$ cm$^{-3}$, respectively. It is concluded that the polaron and bipolaron concentrations in S2 are higher than those in S1, and the oxidation state of S2 is more stable. In addition, from the XPS spectrum (Fig. 3), the content of carbon $C_{\pi-\pi*}$ having delocalizability in the PEDOT chain was obtained. As shown in Table 1, the $C_{\pi-\pi*}$ peak area ratios in S1 and S2 were 1.11% and 3.49%, respectively. It is obvious that the addition of sulfuric

acid to the polymerization system increases the concentration of carbon with delocalization ability in PEDOT:PSS, which makes it possible to increase the carrier concentration in the PEDOT chain.

According to the eqn (2), besides the carrier concentration, the factors affecting the conductivity also include the carrier mobility. Polarons and bipolarons can propagate along PEDOT chains, and their mobilities depend on delocalization over many monomer units.[42]

According to the current general understanding,[40,42,45] for PEDOT chains, a more planar structure means a larger delocalized region of electrons, representing higher carrier mobility. This indicates that a higher quinoid/benzenoid ratio leads to a more planar PEDOT chain structure, which in turn leads to higher carrier mobility. In order to obtain the ratio of the benzenoid and quinoid structures of PEDOT chains in PEDOT:PSS, we tested the Raman spectrum of the sample, as shown in Fig. 6(a). The peak of PEDOT was observed between 1100 cm$^{-1}$ and 1550 cm$^{-1}$. The patterns of peak values at 1100 cm$^{-1}$, 1253 cm$^{-1}$, 1366 cm$^{-1}$, 1435 cm$^{-1}$, 1490 cm$^{-1}$, and
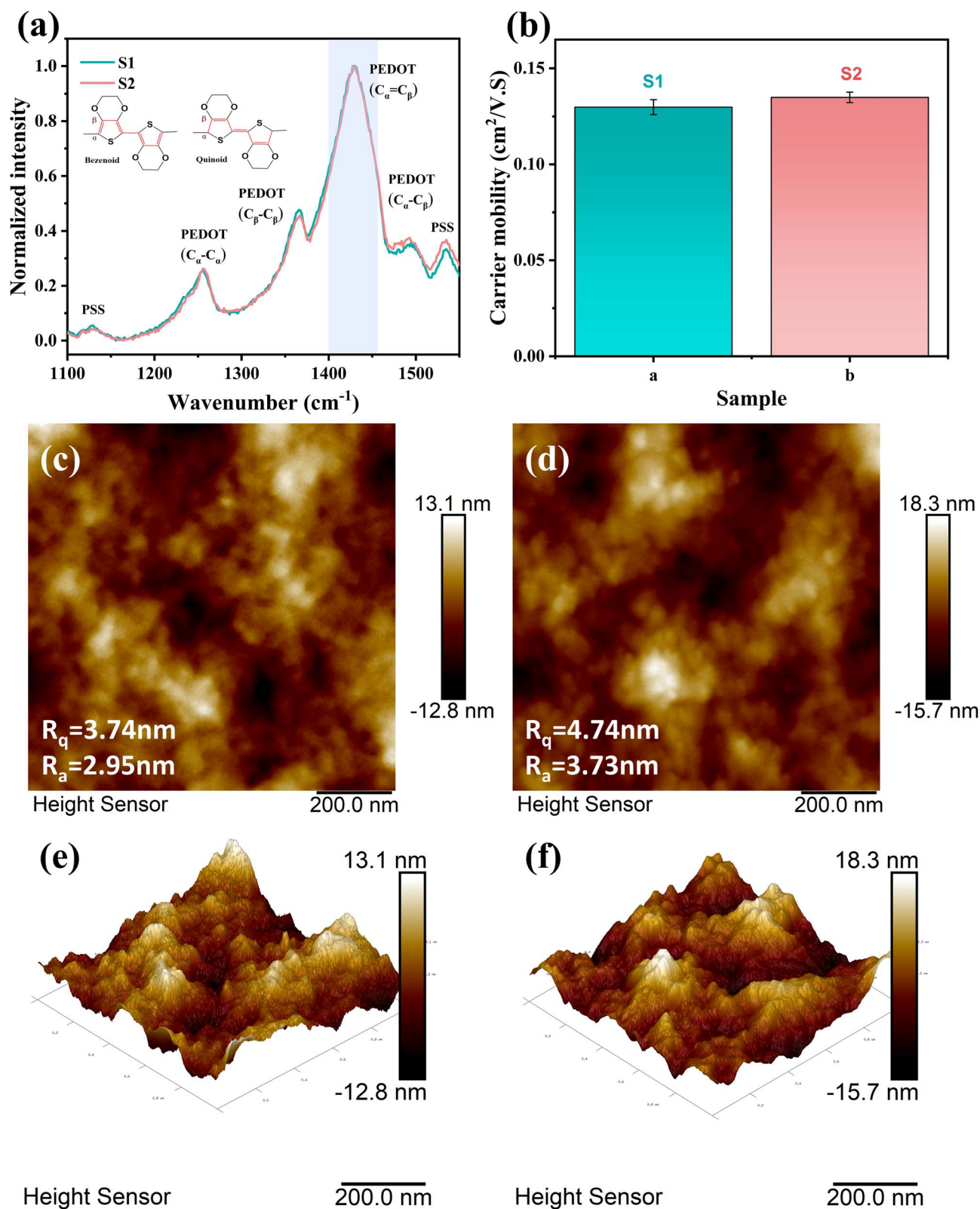
Fig. 6 (a) Raman spectra of the PEDOT:PSS without sulfuric acid and with sulfuric acid. The structural formulas in the figure is benzene structure and quinone structure of PEDOT. (b) Carrier mobility of PEDOT:PSS without sulfuric acid and with sulfuric acid. AFM 2D images of (c) a PEDOT:PSS film without sulfuric acid and (d) with sulfuric acid. AFM 3D images of (e) a PEDOT:PSS film without sulfuric acid and (f) with sulfuric acid.
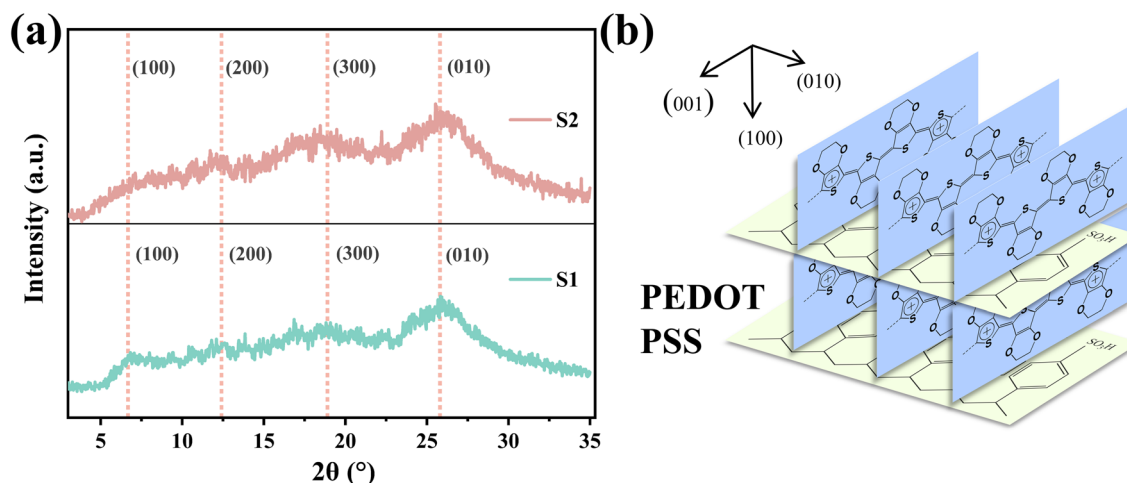
**Fig. 7** (a) XRD patterns of S1 and S2. (b) Molecular packing structure of crystalline PEDOT:PSS. The (100) and (010) lattice spacings are indicated in the figure.

1532 cm$^{-1}$ are indicative of the following: (C–O–C), (C$_\beta$–C$_\beta$ stretch and C$_\beta$–H bend), (C$_\beta$–C$_\beta$ stretch), (symmetric C$_\alpha$=C$_\beta$ (–O) stretch), and (symmetric C=C) in that order, as well as the asymmetric C$_\alpha$=C$_\beta$ (–O) stretch). At 1435 cm$^{-1}$, the symmetric C$_\alpha$=C$_\beta$ (–O) stretch can be divided into two regions derived from benzenoid and quinoid structures, with benzenoid compounds occurring at 1440 cm$^{-1}$ and quinoid compounds occurring at 1410 cm$^{-1}$. The absorption peak at 1435 cm$^{-1}$ narrows or shifts to a lower wavenumber, indicating an increase in quinoid structures.[40,46] We observe that the absorption peak of S2 at this point is only very slightly narrower than that of S1. It can be concluded that the addition of sulfuric acid has little effect on the planarization of PEDOT:PSS. As shown in Fig. 6(b), the carrier mobilities of S1 and S2 measured according to the Hall effect were $1.29 \times 10^{-1}$ cm$^2$ (V s)$^{-1}$ and $1.34 \times 10^{-1}$ cm$^2$ (V s)$^{-1}$, respectively. The difference in carrier mobility between S1 and S2 is not significant. The small difference in carrier mobility is in good agreement with the Raman spectrum. In general, PEDOT chains with more benzenoid moieties are in the form of coiled chains, while PEDOT chains with more quinoid moieties are in the form of extended chains.[47,48] The PEDOT chain will be more regular when it is straightened. Therefore, the PEDOT:PSS film with more PEDOT extended chains will show the state of PEDOT aggregation, which will increase the surface roughness of the film.[49] The surface morphologies of S1 and S2 were measured by AFM. As shown in Fig. 6(c)–(f), the $R_q$ and $R_a$ of S1 were measured to be 3.74 nm and 2.95 nm, respectively; the $R_q$ and $R_a$ of S2 were 4.74 nm and 3.73 nm, respectively. S1 and S2 are only slightly different. And from the height images of AFM, the surface morphology of S1 and S2 films shows no significant difference.

As shown in Fig. 5(d), the conductivities of S1 and S2 were measured to be 5 S cm$^{-1}$ and 28 S cm$^{-1}$, respectively. The conductivity of PEDOT:PSS film was increased by 5.6 times with the addition of sulfuric acid. Due to the small change in carrier mobility, we believe that the increase in conductivity mostly comes from the increase in carrier concentration in the sample.

### 3.3 Crystallinity analysis of PEDOT:PSS

The crystal structure and molecular chain order of S1 and S2 were characterized by X-ray diffraction (XRD) spectra, as shown Fig. 7(a). $2\theta = 6.3°$ corresponds to the lattice plane (100) of PEDOT, associated with the layered overlap of PEDOT and PSS.[23] The plane peak (100) of S2 is obviously weaker than that of S1, which indicates that the sheet stacking distance of S2 increases after adding sulfuric acid, which can be attributed to the growth of PEDOT molecular chains in S2, and is not conducive to the lamellar packing of PEDOT and PSS chains. The diffraction intensities of the two peaks appearing at $2\theta = 12.6°$, $18.9°$ and $25.8°$ correspond to the lattice planes (200), (300) and (010), respectively.[23] The difference of diffraction intensity between S1 and S2 at $2\theta = 12.6°$, $18.9°$ and $25.8°$ is not obvious. The results show that PEDOT in S1 is more regular and easier to crystallize, while the PEDOT chain in S2 is less regular, which can be attributed to the longer PEDOT molecular chain in S2.

In many studies, acid or other organic solvents are usually used to treat PEDOT:PSS to make PEDOT more orderly, so as to obtain higher conductivity.[21–23] In the results of this paper, the conductivity of S1 with better PEDOT regularity is lower, while the conductivity of S2 with worse PEDOT regularity is higher. The improvement of the conductivity of S2 compared with S1 can be attributed to the increase of the molecular weight of PEDOT, which further leads to the increase of the carrier concentration. It can be seen that the change of carrier concentration plays a dominant role in the change of conductivity in this paper, which is better than the effect of PEDOT chain regularity on the conductivity of PEDOT:PSS.

## 4. Conclusion

In this work, we have synthesized and characterized the chemical structure, carrier concentration, and mobility of two PEDOT:PSS dispersions differing by the addition of the protonic acid in the polymerization system with the aim of elucidating its

effect on the chemical structure and conduction mechanism of PEDOT. We show that the introduction of sulfuric acid into the system can inhibit the generation of end groups in PEDOT chains, which helps the chains continue to grow. The carrier concentration and mobility of PEDOT:PSS were studied. With the increase in PEDOT molecular weight, the carrier concentration increases from $1.29 \times 10^{21}$ cm$^{-3}$ to $1.48 \times 10^{21}$ cm$^{-3}$, while the carrier mobility changes only slightly, which increases the conductivity from 5 S cm$^{-1}$ to 28 S cm$^{-1}$.

Furthermore, in addition to the standard approach of indirect qualitative measurement by UV-vis-NIR spectroscopy for detecting the molecular weight of PEDOT, we used the DFT calculations to quantitatively compute the molecular weight of PEDOT and obtained the theoretical value.

## Author contributions

J. G. collected the data. J. G., K. Z., P. L., N. W., S. P., L. W., Y. L., M. H., J. Y., S. Q., Q. F., T. L. and J. X. analysed the data. K. Z. conceptualized and supervised the project. J. G. and K. Z. wrote the original draft.

## Conflicts of interest

There are no conflicts to declare.

## Acknowledgements

## References

1 V. V. Anton, W. Kosala, M. Evangelia, A. Ujwala, Z. Dan, T. Klas, W. A. Jens, B. Magnus, C. Xavier and V. Z. Igor, *Adv. Funct. Mater.*, 2017, **27**, 1700329.

2 Z. Fan and J. Ouyang, *Adv. Electron. Mater.*, 2019, **5**, 1800769.

3 B. Lu, H. Yuk, S. Lin, N. Jian, K. Qu, J. Xu and X. Zhao, *Nat. Commun.*, 2019, **10**, 1043.

4 L. V. Kayser and D. J. Lipomi, *Adv. Mater.*, 2019, **31**, 180613.

5 L. Liu, J. Chen, L. Liang, L. Deng and G. Chen, *Nano Energy*, 2022, **102**, 107678.

6 J. Li, J. Cao, B. Lu and G. Gu, *Nat. Rev. Mater.*, 2023, **8**, 604–622.

7 S. Sandrez, Z. Molenda, C. Guyot, O. Renault, J. Barnes, L. Hirsch, T. Maindron and G. Wantz, *Adv. Electron. Mater.*, 2021, **7**, 2100394.

8 I. Uguz, M. Ganji, A. Hama, A. Tanaka, S. Inal, A. Youssef, R. M. Owens, P. P. Quilichini, A. Ghestem, C. Bernard, S. A. Dayeh and G. G. Malliaras, *Adv. Healthcare Mater.*, 2016, **5**, 3094–3098.

9 X. Wang, Z. Wu, Y. Liu, L. Yin, S. Hou, J. Mao, F. Cao and Q. Zhang, *Adv. Funct. Mater.*, 2023, **33**, 2300886.

10 Z. Wu, X. Wang, S. Hou, Y. Liu, Z. Tang, L. Yin, Y. Qiao, J. Wang, X. Liu, J. Mao, Q. Zhang and F. Cao, *Adv. Opt. Mater.*, 2023, 2301303.

11 J. Friedrich, K. Werner and M. Bavo, *Macromol. Symp.*, 1995, **100**, 169–173.

12 L. Groenendaal, F. Jonas, D. Freitag, H. Pielartzik and J. R. Reynolds, *Adv. Mater.*, 2000, **12**, 481–494.

13 J. Y. Kim, J. H. Jung, D. E. Lee and J. Joo, *Synth. Met.*, 2002, **126**, 311–316.

14 J. Ouyang, Q. Xu, C. Chu, Y. Yang, G. Li and J. Shinar, *Polymer*, 2004, **45**, 8443–8450.

15 M. N. Alexandre, A. J. J. René and K. Martijn, *Adv. Funct. Mater.*, 2008, **18**, 837–966.

16 Q. Wei, M. Mukaida, Y. Naitoh and T. Ishida, *Adv. Mater.*, 2013, **25**, 2757–2866.

17 F. Wu, P. Li, K. Sun, Y. Zhou, W. Chen, J. Fu, M. Li, S. Lu, D. Wei, X. Tang, Z. Zang, L. Sun, X. Liu and J. Ouyang, *Adv. Electron. Mater.*, 2017, **3**, 1700047.

18 L. Valentina, D. Luisa, M. Giovanni, S. Silvia, S. Daniele, L. M. Antonino, T. Antonio and A. P. Rosaria, *Polymer*, 2018, **155**, 199–207.

19 L. Zhang, K. Yang, R. Chen, Y. Zhou, S. Chen, Y. Zheng, M. Li, C. Xu, X. Tang, Z. Zang and K. Sun, *Adv. Electron. Mater.*, 2020, **6**, 1900648.

20 Y. Jia, Q. Jiang, B. Wang, Z. Ma, D. Zhao, N. Zheng, J. Zhou, P. Liu, D. Hu and Y. Ma, *Compos. Commun.*, 2021, **27**, 100844.

21 Y. Xia and J. Ouyang, *Acs Appl. Mater. Interfaces*, 2010, **2**, 474–483.

22 Y. Xia, K. Sun and J. Ouyang, *Adv. Mater.*, 2012, **24**, 2436–2440.

23 N. Kim, S. Kee, S. H. Lee, B. H. Lee, Y. H. Kahng, Y. Jo, B. Kim and K. Lee, *Adv. Mater.*, 2014, **26**, 2268–2272.

24 Z. Zhao, Q. Liu, W. Zhang and S. Yang, *Science China Chemistry*, 2018, **61**, 1179–1186.

25 I. Paulraj, T. Liang, T. Yang, C. Wang, J. Chen, Y. W. Wang and C. Liu, *Acs Appl. Mater. Interfaces*, 2021, **13**, 42977–42990.

26 C. Lo, Y. Wu, E. Awuyah, D. Meli, D. M. Nguyen, R. Wu, B. Xu, J. Strzalka, J. Rivnay, D. C. Martin and L. V. Kayser, *Polym. Chem.*, 2022, **13**, 2764–2775.

27 K. Jooyoung, P. Chanil, I. Soeun, L. Hongjoo and H. K. Jung, *RSC Adv.*, 2019, **9**, 4028–4034.

28 D. M. Joshua and K. P. Christine, *Org. Electron.*, 2014, **15**, 1707–1710.

29 J. D. Morris, D. Khanal, J. A. Richey and C. K. Payne, *Biomater. Sci.*, 2015, **3**, 442–445.

30 J. J. Flores, C. K. Payne and J. D. Morris, *RSC Adv.*, 2017, **7**, 12017–12021.

31 H. F. P. Barbosa, G. D. G. Higuita, F. Günther and G. C. Faria, *Adv. Electron. Mater.*, 2021, **8**, 2100864.

32 S. K. W. L. Andreas Elschner, *PEDOT: Principles and Applications of an Intrinsically Conductive Polymer*, CRC Press, 2011.

33 L. Hongjoo, K. Youngno, C. Hangyeol, L. Jin-geun and H. K. Jung, *RSC Adv.*, 2019, **9**, 17318–17324.

34 H. Cho, W. Cho, Y. Kim, J. G. Lee and J. H. Kim, *RSC Adv.*, 2018, **8**, 29044–29050.

35 S. Zhang, W. Zhang, G. Zhang, Y. Bai, S. Chen, J. Xu, Z. Yu and K. Sun, *Mater. Lett.*, 2018, **222**, 105–108.

36 T. Elena, I. Iryna, S. Jan, Š. Ivana, Z. Alexander, H. Jiřina, P. Jiří, L. Miroslava, V. Nadiia and J. Larysa, *Macromol. Chem. Phys.*, 2020, **221**, 200021.

37 W. E. Richter, A. F. Silva, L. N. Vidal and R. E. Bruns, *Phys. Chem. Chem. Phys.*, 2016, **18**, 17575–17585.

38 J. J. Apperloo, L. B. Groenendaal, H. Verheyen, M. Jayakannan, R. A. J. Janssen, A. Dkhissi, D. Beljonne, R. Lazzaroni and J.-L. Brédas, *Chemistry*, 2002, **8**, 2384–2396.

39 Q. Fu, Y. Li, X. Wang, Q. Li, F. Wang and R. Yang, *J. Mater. Chem. C*, 2020, **8**, 17185–17193.

40 Q. Zhao, R. Jamal, L. Zhang, M. Wang and T. Abdiryim, *Nanoscale Res. Lett.*, 2014, **9**, 557–566.

41 S. S. Zade, N. Zamoshchik and M. Bendikov, *Acc. Chem. Res.*, 2011, **44**, 14–24.

42 S. K. Smita and S. P. Pramod, *Synth. Met.*, 2016, **220**, 661–666.

43 S. Gursel, *Chem. Commun.*, 2005, 5251–5259.

44 C. M. Amb, A. L. Dyer and J. R. Reynolds, *Chem. Mater.*, 2011, **23**, 397–415.

45 R. Nicolas, M. Mohsen, F. F. Juan and Z. Igor, *Comput. Mater. Sci.*, 2020, **179**, 109678.

46 M. S. Cho, Y. Y. Yun, J. D. Nam, Y. Son and Y. Lee, *Synth. Met.*, 2008, **158**, 1043–1046.

47 G. Tian, J. Zhou, Y. Xin, R. Tao, G. Jin and G. Lubineau, *Polymer*, 2019, **177**, 189–195.

48 L. Ouyang, M. J. Jafari, W. Cai, L. E. Aguirre, C. Wang, T. Ederth and O. Inganäs, *J. Mater. Chem. C*, 2018, **6**, 654–660.

49 D. Yun, K. Hong, S. H. Kim, W. Yun, J. Jang, W. Kwon, C. Park and S. Rhee, *Acs Appl. Mater. Interfaces*, 2011, **3**, 43–49.